THE NORTH CENTRAL TEXAS URBAN HEAT ISLAND MAGNITUDE AND ITS RELATION TO SEVERE AND EXTREME DROUGHT

by

LINNEA CLARKE STANDARD

Presented to the Faculty of the Graduate School of

The University of Texas at Arlington in Partial Fulfillment

of the Requirements

for the Degree of

MASTER OF SCIENCE IN EARTH AND ENVIRONMENTAL SCIENCES

THE UNIVERSITY OF TEXAS AT ARLINGTON

May, 2021

Acknowledgements

Foremost I would like to acknowledge my advisor Dr. Arne Winguth for his support, expertise, counseling, and mostly patience. I thank my committee members Dr. Un-Jung Kim and Dr. Hyeong-Moo Shin for their advice and guidance. I am also grateful to Dr. Cornelia Winguth for her critiques and help throughout my research, as well as the Climate Working Group in the Earth and Environmental Science Department at the University of Texas Arlington.

I would like to thank the University of Texas at Arlington for financial support, NSF grant EAR 1636629, and high-performance computing support from Cheyenne (doi:10.5065/D6RX99HX) provided by NCAR's Computational and Information Systems Laboratory, sponsored by the National Science Foundation.

April 28, 2021

Abstract

THE NORTH CENTRAL TEXAS URBAN HEAT ISLAND AND ITS RELATION TO SEVERE AND EXTREME DROUGHT

Linnea Clarke Standard, MS

The University of Texas at Arlington, 2021

Supervising Professor: Arne M. E. Winguth

This study focuses on how summer droughts affect the urban heat island (UHI) in Dallas-Fort Worth (DFW). The nocturnal UHI has been computed by comparing downtown temperature observations to rural temperature measurements under the condition that wind speed is less than 2 m/s, a cloudless sky, and no precipitation. To understand the combined effects of long-term climate change and UHI, trends of temperature anomalies from 1902 - 2019 for Waco and 1900 – 2019 DFW from NOAA COOP were determined relative to a baseline of 1951-1980. The differing trends of these temperature anomalies have been influenced by the UHI (which is larger in the DFW metropolitan area than in Waco) and the higher continentality of the DFW sites. The NOAA Palmer Drought Severity Index (PDSI) was investigated for Climate Zone 3 in Texas and used to isolate years of extreme-severe drought during the month of July and correlated to the UHI magnitude estimates from NOAA COOP and Texas Commission for Environmental Quality (TCEQ). The findings suggest a statistically significant correlation between an increase in the

PDSI and the UHI magnitude for the most current decade from 2011 to 2020, in agreement with the study from Winguth and Kelp (2013) for the previous decade. The reduced latent heat flux under drought conditions can lead increase of the UHI. Under wet conditions the UHI magnitude is below 3°C. The most extreme daily UHI_{mag} of 5.6°C occurred during the severe drought in July of 2011. Population change appears to influence anthropogenic heat flux in the DFW area, however, land surface changes attribute to latent and sensible heat fluxes that affect the UHI magnitude.

Table of Contents

Table of Tables and Figures

Chapter 1

Introduction

This study focused on how drought and freshwater fluxes effect the urban heat island (UHI) in a subtropical climate zone, specifically in North Central Texas which includes the Dallas Fort Worth metropolitan area. In the following, urban heat island characteristics, climate variations and climate change, demographics, and socio-economic concerns are discussed. The urban heat island (Figure 1) is affected by canyon radiative geometry, thermal properties of structures in the city including albedo of surfaces, anthropogenic heat flux, urban greenhouse gases, evapotranspiration of surfaces, and turbulent transfer of heat (Oke et al. 2017). The UHI is defined by the difference between urban surface (T_u) and rural surface (T_r) temperature (Howard 1833; Oke and Maxwell 1975; Runnalls and Oke 2000; Winguth and Kelp 2013). A measure of the urban heat island is its magnitude (UHI_{mag}) defined by the difference in background rural and the urban temperature.

The UHI_{mag} can be estimated as suggested by Oke (1973) as a function of population (P) and wind speed (μ):

$$UHI_{mag} = Tu - Tr = \frac{P^{0.27}}{4.04\bar{\mu}^{0.56}} \qquad (1).$$

However, this aforementioned equation may be not suitable for large, sprawling metroplexes with complex urban development like the DFW area (e.g. Winguth and Kelp 2013) and does not follow the more stringent definition of the nocturnal UHI by Runnals and Oke (2000) which requires calm conditions and clear skies. It is estimated that 80% of the global population now inhabit urban areas, whether that be

industrialized city centers and suburbs or rapidly built and densely packed settlements (Molles 2013). With this increase in urban population, it is of importance to understand how development of urban areas affect latent heat flux within the broader context of global climate change.

While the causes of the urban heat island are complex and varied, changes in land cover that affect the surface energy balance (SEB) of the environment are the root of the issue. The SEB takes place in the atmospheric boundary layer, which is the layer of the troposphere that is influenced by the earth surface, high atmospheric mixing, or turbulence. The upper boundary of this layer is usually characterized by a comparatively stable inversion layer that transitions into a free atmosphere. In urban environments the atmospheric boundary layer forms an internal boundary layer called the urban boundary layer. The energy balance of the urban boundary layer (Oke 1982) incorporates the surface net radiant flux (Q^*), anthropogenic heat flux (Q_F), sensible heat flux (Q_H), latent heat flux (Q_E), and storage (ΔQ_S)

$$Q^* + Q_F = Q_E + Q_H + \Delta Q_S \quad (2).$$

Sensible and latent heat flux are large contributors to the urban and rural energy balance and determining the type and amount of heat lost and/or gained in the environment can be determined using the Bowen's ratio (β) (see Oke 1982)

$$\beta = \frac{Q_H}{Q_E} \quad (3).$$

Bowen's ratio with higher values indicates a reduced water storage, such as an urban environment, or drought. Suburban landscapes can vary greatly depending on irrigation, land cover, and climate. Typical rural environments can have a ratio of 0.5, with urban

landscapes having a ratio of 1.5. Suburban lawns typically have a ratio of 1.0 but may range from 0.25 to 2.5 depending on specific landscapes (Oke 1982).

The temporal and physical structure of urban heat islands vary depending on geographic location and climate of the region. However, for the northern hemisphere the highest UHI magnitude typically occurs during the summer months of June, July, and August (JJA; Ackerman 1985). For areas with spring and fall seasonal precipitation the combination of high summer temperatures and drought may lead to elevated UHI magnitudes and nocturnal temperatures for urban residents. Urban areas have increased land cover percentage of impermeable surfaces and this combined with drought conditions usually results in an overall reduction of water in the ecosystem. The UHI generally appears to be strongest just after sunset (Figure 1) during calm and clear weather conditions. There is often a small negative urban heat island during the day for many cities (Oke and Maxwell 1975; Oke 1982; Runnalls and Oke 2000). Daily weather conditions of wind direction, wind speed, and cloud cover can affect the UHI magnitude (Brandsma and Wolters 2012; Oke 1982; Winguth and Kelp 2013). When cloud cover and/or wind speed increases the nighttime maximum UHI is closer to sunset and the magnitude is reduced significantly (Ackerman 1985) and, increased wind speed reflects a negative logarithmic relationship with the UHI magnitude (Oke 1976). Sunrise generates a sensible heat flux and temperatures reach their maximum at mid-afternoon, however, at sunset rural areas cool off at a faster rate than urban areas due to increased evaporation and transpiration. Land use has been shown to affect temperature profiles, especially in the urban canopy layer, with the urban rate of warming and cooling being generally smaller than rural rates (Oke 1982). There are

distinct temperature gradients between the urban and rural boundaries with weaker gradients as the city center is approached, these gradients also occur around city parks and bodies of water, creating cool spots (Figure 1; Oke and Maxwell 1975; Oke 1982; Runnalls and Oke 2000). The Oklahoma City UHI_{mag} is strongest in the downtown area with high median building height and little green space (Hu et al. 2016). When assessing the rural temperature, a location should be chosen that is within the same climate zone and ecosystem but at a distance that is not affected by the urban plume (Liu and Niyogi 2020). The urban plume is a boundary layer that can increase rural temperatures downwind through advection and elongate temperature gradients (Figure 1). The urban heat island has been shown to influence the microclimate of the urban ecosystem with days over 32.2ºC increasing and days below 0ºC decreasing (Schmidlin 1989). The dominant factor controlling the UHI is latent heat flux and evapotranspiration of water from the surface to the atmosphere (Oke 1982). Surfaces with low moisture content have a lower heat flux, either due to low soil moisture from drought or impermeable surfaces, and therefore a larger urban heat island magnitude (Oke et al. 2017). Seasonal variation in precipitation, especially among subtropical and temperate cities, is strongly associated with an increase in the nocturnal UHI. Drier conditions exacerbate this association of the increasing nocturnal urban heat island magnitude (Roth 2007). Periods of drought during the summer month in July has been shown to increase the UHI magnitude in the DFW metroplex, especially the intense and prolonged drought of 2011 (Winguth and Kelp 2013).

The magnitude of the UHI_{max} in North Central Texas is dependent on weather patterns, elevation, and land cover influencing the region. The maximum UHI (UHI_{max}) is

the strongest UHI_{mag} for a given area on a given day (Zhang et al. 2019). Texas climate patterns are mainly affected by air masses from the Rocky Mountains, Central Great Plains, and the Gulf of Mexico. Generally, temperatures in Texas increase southward due to greater insolation, however, there are hot and cool spots due to geographic formations (Figure 2). Temperature variation increases as we move further inland from the Gulf of Mexico, due to the moderating effect of oceanic winds and air mass temperatures. This increase in continentality between Houston and Dallas-Fort Worth exemplifies this temperature variation (Hu and Xue 2016). Precipitation decreases westward with desert and high plains ecosystems beginning to dominate (Figure 2). May and September have the highest median rainfall for the North Central Texas, and the projected temperature rise of 2.22 °C by 2060 could further tax the hydrologic cycle in the region (Nielsen-Gammon 2011). North Central Texas is classified as Class C (Temperate) and subclassified as a Humid Subtropical Climate in the Köppen-Geiger system. The average July temperatures for the North Central Texas are between 34°C – 36°C and average precipitation in July is around 50 mm per month (Neilsen-Gammon 2011). Global climate (IPCC 2013) and land cover change in the future may lead to a change in the climate zone.

The UHI may also be influenced by natural fluctuations that are caused by interannual to millennia variations (e.g., El Niño Southern Oscillation (ENSO), Atlantic Multidecadal Oscillation (AMO), and/or volcanic eruptions) (Foster and Rahmstorf 2011; Khedun et al. 2014; Seager et al. 2014). For example, warmer than normal temperatures, associated lower soil moisture, and droughts in North Central Texas are correlated to La Niña or positive phases of the ENSO (Seager et al. 2014). During La

Niña, eastern equatorial upwelling is amplified due to a more intense high pressure over the subtropical South Pacific Ocean, thus leading to cooler than normal sea surface temperatures. During La Niña conditions annual precipitation over North Central Texas decreases up to 76.2 mm, however, mainly during winter to spring season. La Niña is weakest during the summer months of June, July, and August and therefore its effect on summer precipitation rates is weaker in the southcentral U.S. (Kurtzman and Scanlon 2007). Correlation of UHI in the DFW area with ENSO exist (Figure 13) and is linked to shifting of the subtropical jet stream. These subtropical atmospheric changes are linked to a strengthening of the Hadley cell circulations during El Niño and a weakening during La Niña respectively. The input of heat, El Niño, from the equatorial Pacific drives this circulation and a reduction of that oceanic heat, La Niña, would weaken Hadley cells (Bjerknes 1969). This atmospheric circulation pattern is directly related to the strength of the subtropical jet stream, which in turn, influences precipitation rates in North Central Texas. A weakened subtropical jet stream directs precipitation north along the U.S. Pacific Northwest coast, and subsequently drought occurs in the interior United States southwest. Multiple oscillation events occurring simultaneously exacerbate or dampen teleconnections, for example a negative phase of the Pacific Decadal Oscillation (PDO) and La Nina phase of ENSO would strengthen teleconnections (McCabe and Dettinger 1999). The lag-time of equatorial oceanic forcing to subtropical atmospheric changes in North American can be measured in days not weeks or months (Bjerknes 1969).

Climate change is expected to increase global precipitation (Wentz et al. 2007), and regional extreme precipitation events for the mid-latitudes whereas subtropical regions will become more arid (IPCC 2014). Figure 3 from the Goddard Institute for

Space Studies (GISS) outlines the long-term anthropogenic-induced climate change superimposed on natural interannual to decadal fluctuation.

North Central Texas, defined by the National Weather Service (NWS), contains 44 counties that encompass just over 141,476 km^2 and includes the highly populated Dallas, Tarrant, Denton, and Collin counties. The aforementioned counties are among the top ten fastest growing in the state with a projected population growth of just over 6 million people from 2010 – 2050 (You et al. 2019). The defined region has an average growth rate of 14.6% and a population change of just over 1.5 million from 2000 – 2010. The four most populated counties have an average population growth rate of 36.0%, according to the U.S. Census Bureau (Figure 5). If growth rates remain constant North Central Texas population may reach over 9.5 million in 2019 and could reach 17 million by 2050. Dallas and Tarrant counties have the highest population densities of 1049 and 808 people per km^2 in 2010 and are projected to reach 1331 and 1620 people per km^2 by 2050 (U.S. Census Bureau 2020).

With the increase in urban populations globally, it is important to understand the socio-economic impacts of UHI. These higher urban temperatures can increase photochemical reaction such as formation of ozone due to emission of nitrogen oxides (NOx) and Non-methane hydrocarbons (NMHC). Increases in ozone concentration in the troposphere lead to respiratory disorders, in particular for the vulnerable population. In addition, the UHI requires more energy for cooling of buildings especially in the tropical and subtropical climates. For example, a 2 °C UHI may increase residential cooling that would result in additional CO_2 emission of 2 million tons for the state (Roxon et al. 2020). The increased cost of residential cooling in Texas for such a

temperature change is ~$400 million (Roxon et al. 2020). In cities with colder climates the UHI may reduce heating cost in the winter.

The nocturnal stable boundary layer may accumulate pollutants. Rise in nocturnal temperatures may also exacerbate the formation of secondary pollutants and a lower mixing layer further degrades air quality. For example, rise in PM_{10} concentration appear to be inversely correlated to the urban boundary layer height (Wagner and Schäfer 2017). Superimposed of the UHI is global climate change that lead to increase of heat waves and extreme precipitation events (IPCC 2013).

Chapter 2

Objectives

This study aims to determine the ongoing relationship between magnitude of the UHI_{mag} in North Central Texas and drought (Figure 4). Data from the Texas Commission for Environmental Quality (TCEQ) Continuous Ambient Monitoring Stations (CAMS) and NOAA Palmer Drought Severity Index (PDSI) for the month of July has been gathered to determine if the correlation between UHI_{mag} and latent heat flux is changing.

In this study, we focused on following objectives:

1. How does climate change and extreme weather like droughts affect the urban heat island in North Central Texas?
2. How sensitive is the UHI to changes in climatic variables (e.g., heat and freshwater fluxes)?
3. How does spatial temperature distribution change with PDSI?

Here we reassess findings from a previous study that suggested a correlation between precipitation rates, prolonged drought conditions, and the magnitude of the UHI (Figure 4; Winguth and Kelp 2013) with new meteorological measurements from the last decade. A reduction in latent heat flux could be a major contributor to the rise in the UHI_{mag} for the study area.

Chapter 3

Methodology

3.1 Study Site

The North Central Texas climatic region contains 44 counties that encompass just over 141,476 km^2 and includes the densely populated Dallas, Tarrant, Denton, and Collin counties. The National Weather Service (NWS) Cooperative Observer Program (COOP) stations are located at the Dallas-Fort Worth (DFW) international and Waco regional airport with the climatological station to be at the DFW airport. The 2 NWS stations will be used for decadal climatic comparisons. In addition, 33 active CAMS from TCEQ were used in this study (Table 1). The Kaufman station was utilized as the rural location while the Dallas-Hinton station was used for urban measurements (Figure 6). The Kaufman station is sufficiently surrounded with a suburban lawn environment including the local high school to east. It is 73.8 km from downtown Dallas, however, a nearby road and high school complex could attribute to a bias. It is also located to the SE of the metropolitan area which is characterized by the highest soil moisture as described by NOAA satellite and in situ soil moisture estimates (Kalnay et al. 1996). The recommended distance of two times the length of the metropolitan footprint from the geographical center (Liu and Niyogi 2020) cannot be achieved due to the size of the DFW metroplex and absence of TCEQ and NOAA COOP stations in that perimeter. Continuous Ambient Monitoring Station (CAMS) 60 from the Texas Commission of Environmental Quality (Table 1) was selected as a downtown reference station based on analysis from Winguth and Kelp (2013). The later site does not have a significant reduction in skyview factor (>0.7) that would skew diurnal measurements (Winguth and

Kelp 2013). Although CAMS 312 is closer to downtown Dallas, it is located on a rooftop and thus may misrepresent measurements due to its screen height and surrounding surface.

3.2 Meteorological Data

The NWS COOP stations at DFW airport (KDFW) and Waco airport (KACT) were used to gather historical climatological temperature and precipitation data to establish long term climate patterns for the area. Anomaly graphs were created using MATLab and a baseline average of 1951-1980 was used in accordance with Figure 3. A 25% weighted scatterplot smoothing (LOWESS) was applied to remove the high frequency noise and outliers (Cleveland 1979) within the data following the approach of Hansen et al. (1999). NWS stations were used to isolate times in July when weather conditions are calm, no precipitation and less than 2 m/s wind speed.

The CAMS (Table 1) were used to compute UHI_{mag} and are manufactured and installed by Climatronics Corporation, with temperature sensors mounted 10 m above the base of the structure. Climatronics Corporation has since been acquired by Met One Instruments incorporation, however, CAMS were set-up prior to this acquisition. Geographic Information Systems software (ArcGIS) was used to interpolate data and estimate points between stations via spatial analysis.

The Palmer Drought Severity Index (PDSI; Palmer 1965) updated by NOAA, for July was utilized to ascertain drought severity for the North Central Texas region (NOAA

2020). Table 2 shows the PDSI classifications, ranging from extreme drought to extremely moist, and will be compared to reference years in this study.

Volumetric soil moisture plots were created using the NCEP/NCAR Reanalysis 1: Surface Flux tool. Soil moisture data at a depth of 0-10 cm averaged between 16:00 and midnight for the date which the nocturnal UHI will be measured was obtained. The difference between the Kaufman and Dallas-Hinton stations were calculated to ascertain any correlation between soil moisture and the UHI_{mag}. The years plotted are 2011, 2018, 2014, and 2016, which correspond to extreme drought, severe drought, near normal, and extremely moist conditions, respectively. NCEP Reanalysis data have spatial resolution of T62 (or 2° x 2°).

3.3 Urban Heat Island Measurement

The urban heat island magnitude was determined using the following equation $UHI_{mag} = T_u - T_r$ from Oke (1982), whereas T_u is the temperature at the designated urban station and T_r is the temperature at the designated rural station. Magnitude will be computed at 21:00 CST to avoid synoptic sea-breeze fronts from the Gulf of Mexico (Hu and Xue 2016), and conditions as defined in Runnalls and Oke (2000). The elevation between the rural and urban stations is 1.5m, therefore lapse rate was not calculated.

3.4 Spatial Distribution of the Temperatures

ESRI ArcGIS 10.8.1 data were applied to assess the spatial distribution of temperature and temperature deviation from CAMS 71 across the DFW metroplex. Note

that the UHI_{mag} between Kaufman and Dallas-Hinton TCEQ CAMS was estimated for nighttime 21:00, however wind speeds may have exceeded 2 m/s for some TCEQ CAMS over the area of interest. The data were statistically spatially interpolated between the TCEQ stations by using the ArcGIS semi-variogram Kriging-spherical tool with area weights inferred from map pixel count (Hu et al. 2016). The interpolation area rose from ~ 37,000 km^2 to ~47,500 km^2 in year 2012 due to increased number of TCEQ stations.

Chapter 4

Results

In the first step, we compiled the temperature and precipitation trends from NWS COOP climatological stations of DFW airport and Waco regional airport. The annual average baseline temperatures are 18.7°C for the DFW station and 19.4°C for Waco Station. Those averages rose to 19.7ºC and 19.8ºC with an 5.3% rise in DFW airport and 1.65% rise in Waco in the last 20 years (Figure 7). Analysis of seasonal change indicate similar trends for all seasons (Figure 8).

The average decadal climatic precipitation increased by 1.69% and decreased by -0.48% over the period from 1900 to 2019 for the DFW airport and Waco station, respectively (Figure 9). Average precipitation for the baseline period from 1951 – 1980 is 795.1 mm for the DFW airport station and 786.2 mm for the Waco station are analogous to Figure 2.

Analysis of precipitation data, at DFW airport station, suggests that the most substantial increase occurred during the winter months (55.1 mm per decade) and during the summer months (29.5 mm per decade). Precipitation in spring and fall also rose to 10.7 mm per decade and to 23.7 mm per decade respectively (Figure 10).

The month of highest average temperature and lowest precipitation rates at the DFW airport COOP station occurred during the summer months (JJA; Figure 11). There is a sufficient correlation between extreme July temperature and droughts in North Central Texas (Figure 12). Note that 2006 and 2011 have similar PDSIs but temperature was in 2011 ~1.2ºC higher because of the pre-existing drought condition during that year. Increase in drought leads to a reduce latent heat flux and enhanced

sensible heat fluxes, thus amplifying the surface air temperatures. A relationship with ENSO events and extreme summer drought exists in La Niña years whereas extreme moist conditions are correlated to El Niño years during the same period (Figure 13).

The volumetric soil moisture fraction, the volume ratio of the soil that contains water, of Kaufman exceeds that of Dallas-Hinton (Figure 14) for the same time interval used for the analysis of the UHI_{mag}. Difference in volumetric soil moisture fraction between these stations is largest during the extreme drought of 2011. Note, the coarse resolution of the NCEP Reanalysis data limit the interpretation. Figure 15 indicates a correlation between the difference in volumetric soil moisture fraction and UHI_{mag} with most extreme differences for the year 2011 (Figure 15).

The average UHI for July 2012 is positive from 16:00 to 7:00 CST and peaks between 21:00 and 23:00 CST. The negative UHI last from 7:00 to 12:00 CST and 14:00 to 14:30 CST (Figure 16) that is related to convection during the daytime (see Winguth and Kelp 2013). There is also a difference in the rate and degree of cooling between the Kaufman (CAMS 71) and Dallas-Hinton (CAMS 60) stations linked to higher soil moisture content in the rural site compared to the downtown station (see Winguth and Kelp 2013). The monthly temperature difference variability between urban and rural sites for July is linked to cloud cover and wind speed (Figure 17). This curve does represent the magnitude of the UHI. Note that diurnal variability in Figure 16 is the predominant signal in monthly time series of Figure 17.

Note, that during the extreme drought in year 2011 greatest differences in temperature between urban (34°C) and rural stations (27°C) are 7°C (Figure 18a) whereas differences in year of severe drought in year 2018 and normal conditions in

2014 are 5°C (Figure 18d and 18b). During the extremely moist year of 2016 temperature difference is 6°C (Figure 18c). Figure 19a displays the temperature difference relative to the Kaufman Site. In 2011 maximum temperature difference between the urban area and this station (Figure 19a) is ~4°C (consistent to estimates of Winguth and Kelp (2013). The percentage of area exceeding 30°C is greatest in 2018 at ~75% of the total area whereas in 2011 only ~65% and in 2016 ~60% of the entire area exceeded temperatures of 30°C (Table 3). The increase in area in 2018 relative to 2011 could be partially attributed to the rapid increase in urban development. Note that in 2014 only 33% of the surface area had temperatures above 30°C. In 2011, 43% of the area had a temperature difference of >3°C relative to the Kaufman station. In years 2014, 2016, and 2018 these areas (2%, 5%, and 3% respectively) were substantially smaller (Table 3). The UHI_{max} for the last 10 years (2020-2011) has an average UHI_{mag} of 4.0 °C per year. If we discount the extreme value from 2011 the average UHI_{mag} is 3.8 °C per year.

Pearson's correlation of the UHI with the PDSI are comparable to Winguth and Kelp (2013) with similar r values, ρ values, and slope. 2011 has the highest UHI_{mag} of 5.61°C, while 2018, 2014, and 2016 have UHI_{mag} of 4.44°C, 4.11°C, and 3.56°C. The lowest UHI_{mag} occurred during 2019 with 3.17°C. The UHI magnitude and PDSI is highly inversely correlated with an r value of -0.84.

Chapter 5

Discussion

This study aims to compare the UHI magnitude of the most recent decade from 2011 to 2020 with previous studies (see Winguth and Kelp 2013). Urban heat islands have a characteristic microclimate that effects the regional climate variability. The UHI magnitude of DFW is smaller than that of Phoenix, Arizona, because of higher humidity, but larger than that Houston due to the continentality. The global land ocean temperature rate of increase, from 1981 to 2020, is 0.18ºC per decade (NOAA 2020). The temperature trend for Waco Station is similar to the global trend (0.16ºC per decade) during the same period whereas that for the DFW airport is 0.55ºC per decade which is 3x higher compared to the Waco station. The difference in these trends is related to the continentality and the increase in the UHI_{mag} in the DFW metroplex (GISS 2020; Nielsen-Gammon 2011). In addition, the larger UHI in the DFW area could lead to lower soil moisture and lower precipitation. Note that the arid UHI_{mag} of Mexico City is comparable that of the DWF during drought conditions which is linked the lower latent heat flux and enhanced sensible heat fluxes (Roth 2007). This study utilized statistical analysis via kriging interpolation to determine the spatial extent of the urban heat island. However, this method is limited due to available TCEQ CAMS and does not consider the dynamics of the atmosphere (as for example done by data assimilation using a weather model (Kalnay et al., 1996). However, findings from spatial analysis in this study is agreeable with previous studies (Hu and Xue 2016; Winguth and Kelp 2013). Among the various

heat fluxes, latent heat flux appears to be of importance to estimate the UHI_{mag}. The maximal UHI during drought is influenced by climate variations such ENSO (La Niña) events (Figure 13) or warm phases of the Atlantic multidecadal oscillation (Hoerling et al. 2013). How these osillations are influenced by future climate change remains controversial. Analysis of climate prediction suggest that precipitation rates for North Central Texas may increase with a higher likelyhood of extreme precipitation events and droughts (IPCC 2013; Jiang and Yang 2012; Nielsen-Gammon 2020; Romero-Lankao et al. 2014). The more extreme events may effect reservoirs as occurred for example during the 2011 drought (Nielsen-Gammon et al. 2020).

Uncertanty exists in this study due to differnent screen heights in the obervations, accuracy of the observations, and local affects near the measurements that can affect the heat flux terms.

Chapter 6

Conclusions and Future Perspectives

As weather extremes continue to increase with the advancement of climate change it is important to continue monitoring the effects of extreme to severe drought on the anthropogenic induced urban climate. This study suggests the relationship between the UHI is highly variable and thus the differing contributing factors of urban heat islands need to be evaluated. This could be achieved by increasing monitoring systems, in particular rural areas to improve and better assess the spatial distribution of the UHI. Land cover changes have altered the heat fluxes, in particular the latent heat flux, and influenced the UHI over the recent decades. These processes are not considered in equation (3). Increasing growth of the DFW metroplex and associated changes in land cover will likely contribute to more extreme heat waves and changes in water availability in North Central Texas, particularly during serve droughts.

Future research should consider the discussion of individual changes in sensible and latent heat flux (eq. 3) due to increases in urbanization and suburbanization along with climate change. In addition, the changes in ecosystems due to the UHI and climate change and associated climate feedback need to be addressed. For instance, increase in aridity may lead to shift in soil moisture, vegetation types and latent and sensible heat fluxes. Also, increases in surface reflectivity by a decline in native vegetation under more severe drought may need to be explored. Changes in precipitation rates and extremes, alter the plant hardiness zones. Land use GIS layers from the National Land Cover Database could be utilized with spatial analysis temperature interpolation to interpret any relationships with land cover change and heat islands within the DFW

metroplex. A land use composition model or land surface model (see Lawrence et al., 2019) as part of an earth system model may be useful to estimate complex processes associated with land surface changes. Comparisons of regional climate simulations with other cities in the subtropical climate zone may be also desirable (see Hu et al., 2016).

Tables

Table 1: Amended TCEQ CAMS used for data retrieval (Winguth and Kelp 2013). CAMS 60 will be used as urban, while CAMS 70 will be used as rural reference for UHI magnitude measurements.

CAMS	LOCATION	LATITUDE	LONGITUDE	ELEVATION	IDENTIFIER	ACTIVATION DATE	LCZ
0013	Fort Worth Northwest	32° 48' 21"	-97° 21' 24"	203.0	FWMC	1-Jan-75	9*
0017	Keller	32° 55' 21"	-97° 16' 56"	254.0	KELC	11-Feb-81	9
0031	Frisco	33° 7' 57"	-96° 47' 11"	232.0	FRIC	7-May-92	9
0052	Midlothian OFW	32° 28' 55"	-97° 1' 37"	195.0	MDLO	7-Nov-94	C
0056	Denton Airport South	33° 13' 9"	-97° 11' 47"	183.0	DENT	16-Feb-98	9*
0060	Dallas Hinton	32° 49' 12"	-96° 51' 36"	126.5	DHIC	1-Jan-86	8
0061	Arlington Municipal Airport	32° 39' 23"	-97° 5' 19"	183.0	ARLA	17-Jan-02	9*
0063	Dallas North No. 2	32° 55' 9"	-96° 48' 31"	190.8	DALN	2-Nov-98	9
0069	Rockwall Heath	32° 56' 11"	-96° 27' 33"	168.0	RKWL	8-Aug-00	9
0070	Grapevine Fairway	32° 59' 3"	-97° 3' 49"	165.0	GRAP	4-Aug-00	C
0071	Kaufman	32° 33' 54"	-96° 19' 4"	128.0	KAUF	11-Sep-00	9
0073	Granbury	32° 26' 32"	-97° 48' 13"	226.0	GRAN	9-May-00	8
0075	Eagle Mountain Lake	32° 59' 16"	-97° 28' 38"	241.0	EMTL	6-Jun-00	C
0076	Parker County	32° 52' 8"	-97° 54' 21"	347.0	WTFD	26-Jul-00	C
0077	Cleburne Airport	32° 21' 13"	-97° 26' 12"	250.0	CLEB	10-May-00	9*
0088	Decatur Thompson	33° 13' 18"	-97° 35' 4"	327.0	DECT	6-Aug-10	9
0312	Convention Center	32° 46' 27"	-96° 47' 52"	145.1	DACC	1-Jan-79	8
0402	Dallas Redbird Airport Executive	32° 40' 35"	-96° 52' 19"	206.0	REDB	1-Jan-95	9*
1006	Greenville	33° 9' 11"	-96° 6' 56"	161.0	GRVL	20-Mar-03	9
1007	Flower Mound Shiloh	33° 2' 45"	-97° 7' 48"	194.0	FLMS	27-Oct-10	9
1008	Johnson County Luisa	32° 28' 11"	-97° 10' 9"	209.0	LUIS	23-Nov-10	9
1009	Everman Johnson Park	32° 37' 16"	-97° 17' 25"	204.0	EJPK	28-Jun-11	9
1010	Frisco Eubanks	33° 8' 41"	-96° 49' 44"	198.0	FREB	15-Jan-95	9
1013	DISH Airfield	33° 7' 51"	-97° 17' 52"	667.0	DISH	31-Mar-10	9*
1032	Pilot Point	33° 24' 38"	-96° 56' 41"	201.0	PIPT	4-Apr-06	9
1037	Waco Mazanec	31° 39' 11"	-97° 4' 15"	143.0	WAMA	16-Apr-07	C
1044	Italy	32° 10' 31"	-96° 52' 13"	165.0	ITLY	21-Aug-07	9
1051	Corsicana Airport	32° 1' 55"	-96° 23' 57"	128.0	CRSA	16-Jun-09	9*
5007	Arlington Municipal Airport	32° 39' 50"	-97° 5' 45"	183.0	KGKY	22-Jan-03	9*
5008	Denton Airport South	33° 12' 22"	-97° 11' 56"	183.0	KDTO	22-Jan-03	9*

Table 2: NOAA Classifications for the Palmer Drought Severity Index

Palmer Drought Severity Index Classifications						
Drought			**Normal**	**Moist**		
Extreme Drought	Severe Drought	Moderate Drought	Near Normal	Unusual Moist Spell	Very Moist Spell	Extremely Moist Spell
-4.0 or less	-3.0 to -3.9	-2.0 to -2.9	-1.9 to 1.9	2.0 to 2.9	3.0 to 3.9	4.0 to 4.9

Table 3: Estimated areas based Kriging interpolation from TCEQ CAMS locations (see text) , areas above 30°C , and with a UHI > 3°C relative to the TCEQ CAMS station in Kaufman. Note that the interpolation area rose in 2012 because of an increase in the number of TCEQ stations.

Year	***Total Interpolated Area [km]***	***Area > 30°C [km]***	***UHI area > 3°C [km]***	***Area > 30°C [%]***	***UHI Area > 3°C [%]***
2011	37,100	24,220	15,886	65.28	42.82
2014	47,513	15,914	1,164	33.49	2.45
2016	47,513	28,727	2,312	60.46	4.87
2018	47,513	35,720	1,410	75.18	2.97

Figures

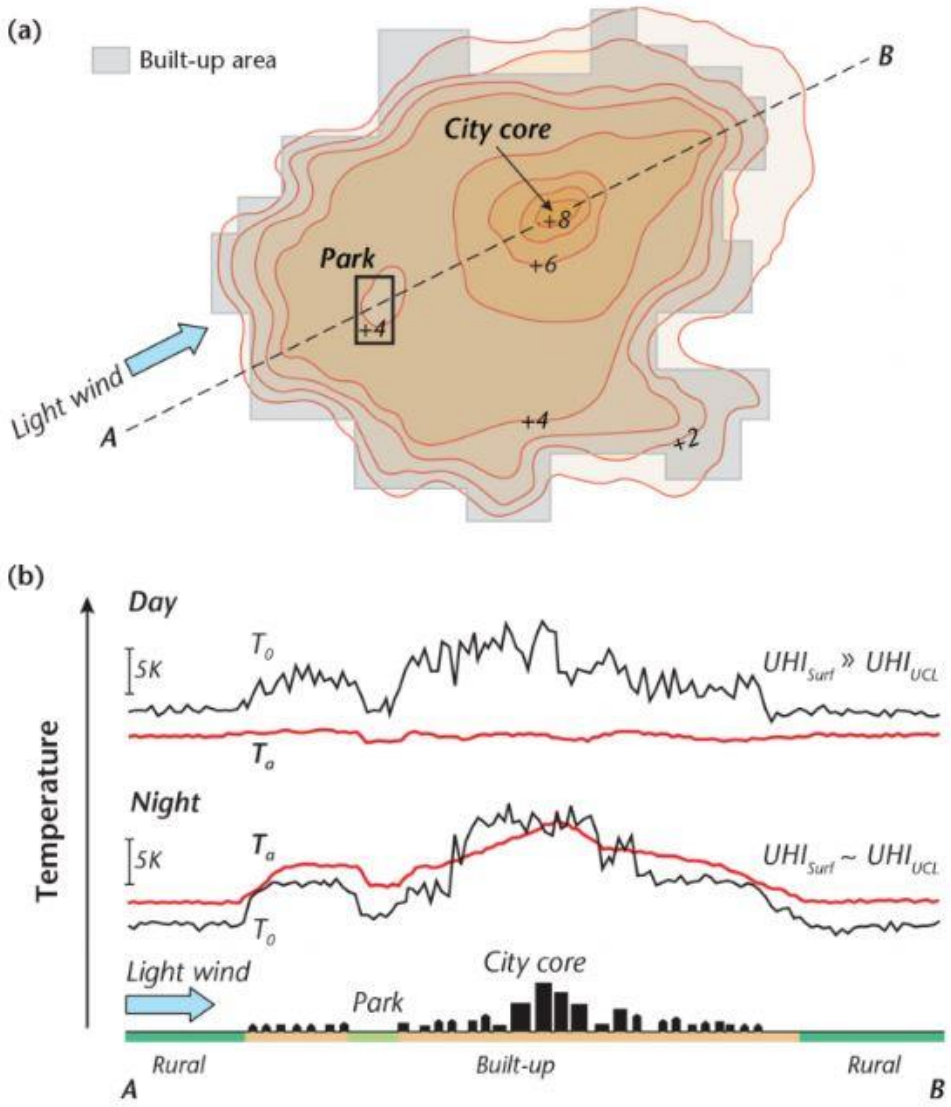

Figure 1: a) Surface temperatures at screening level with ideal conditions over a relatively flat hypothetical city. b) Diurnal and nocturnal surface temperature patterns with T_a being the air temperature and T_0 the surface temperature (Oke et al. 2017).

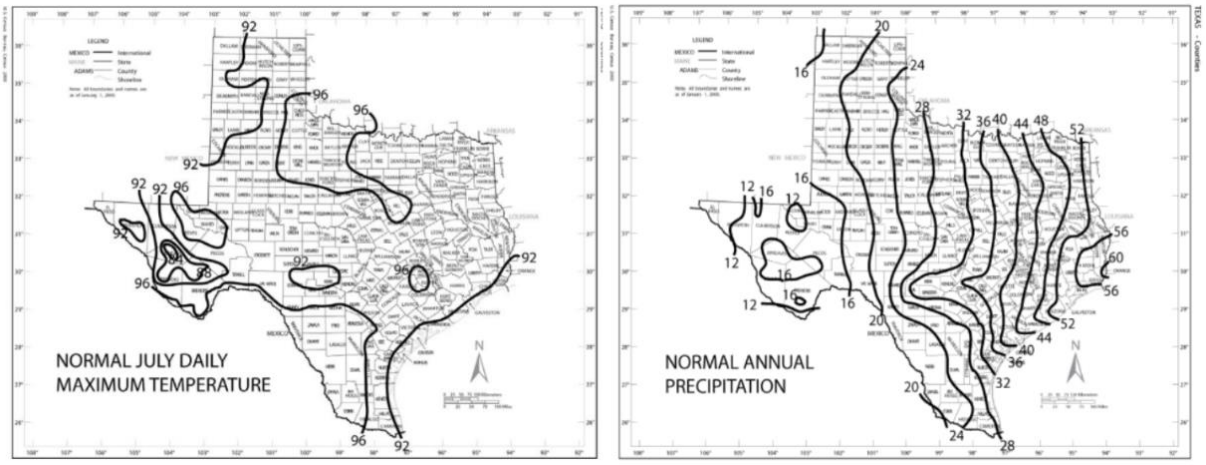

Figure 2: Temperature (ºF) and precipitation (in) patterns for Texas from 1971 – 2000 (Neilsen-Gammon 2011).

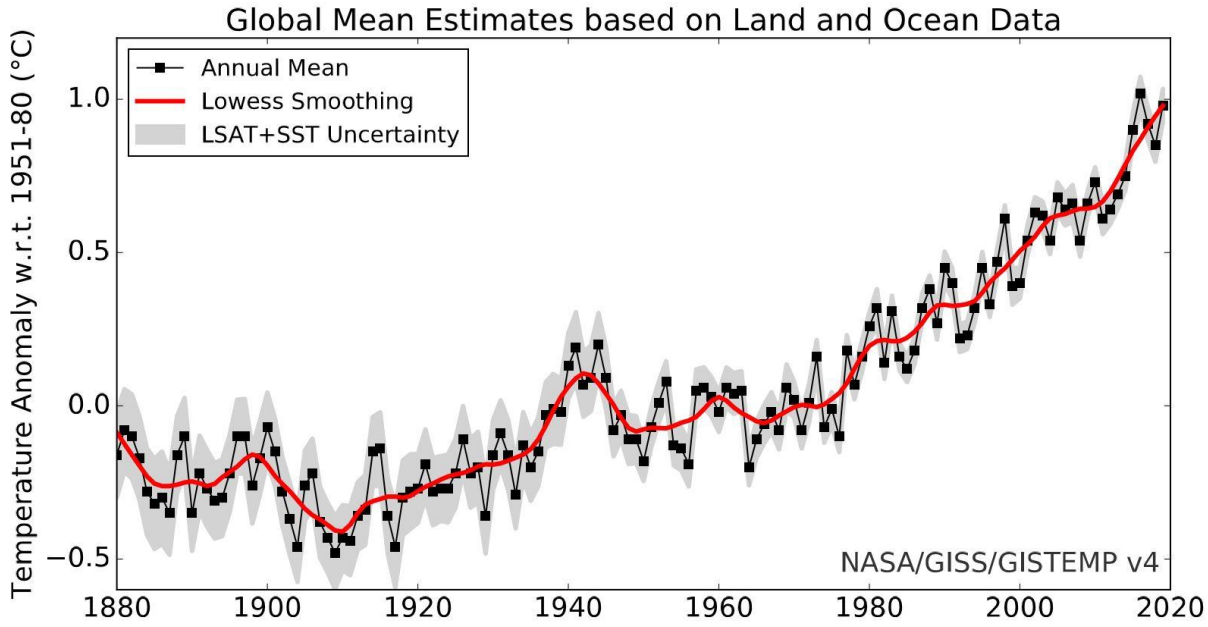

Figure 3: Global surface air temperature anomalies from NASA/GISS (black) with uncertainties of Land and sea surface temperature (grey; 95 confidence interval) and 5-year LOWESS smoothing (with 7% span) relative to a 1951-1980 baseline (Courtesy NASA/GISS).

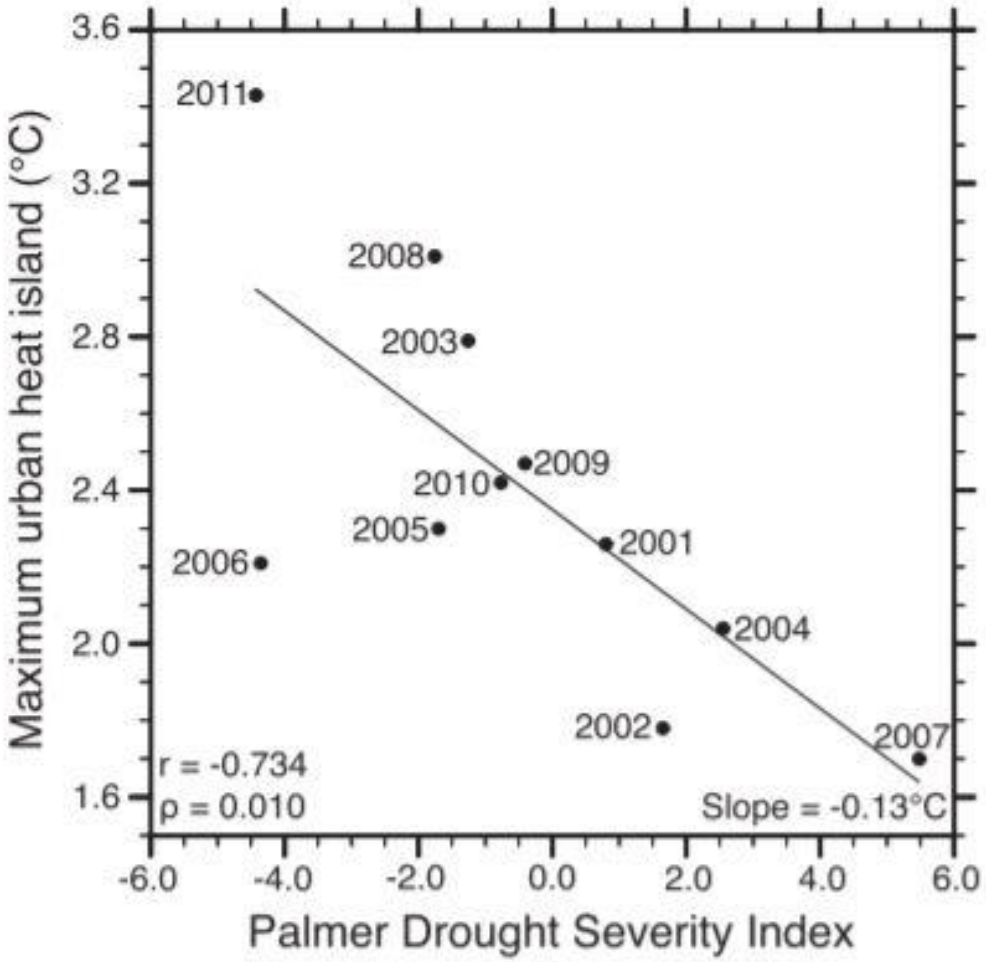

Figure 4: Palmer Drought Severity Index (PDSI) and UHI magnitude for TCEQ Kaufman and Dallas Hinton stations (Winguth and Kelp 2013).

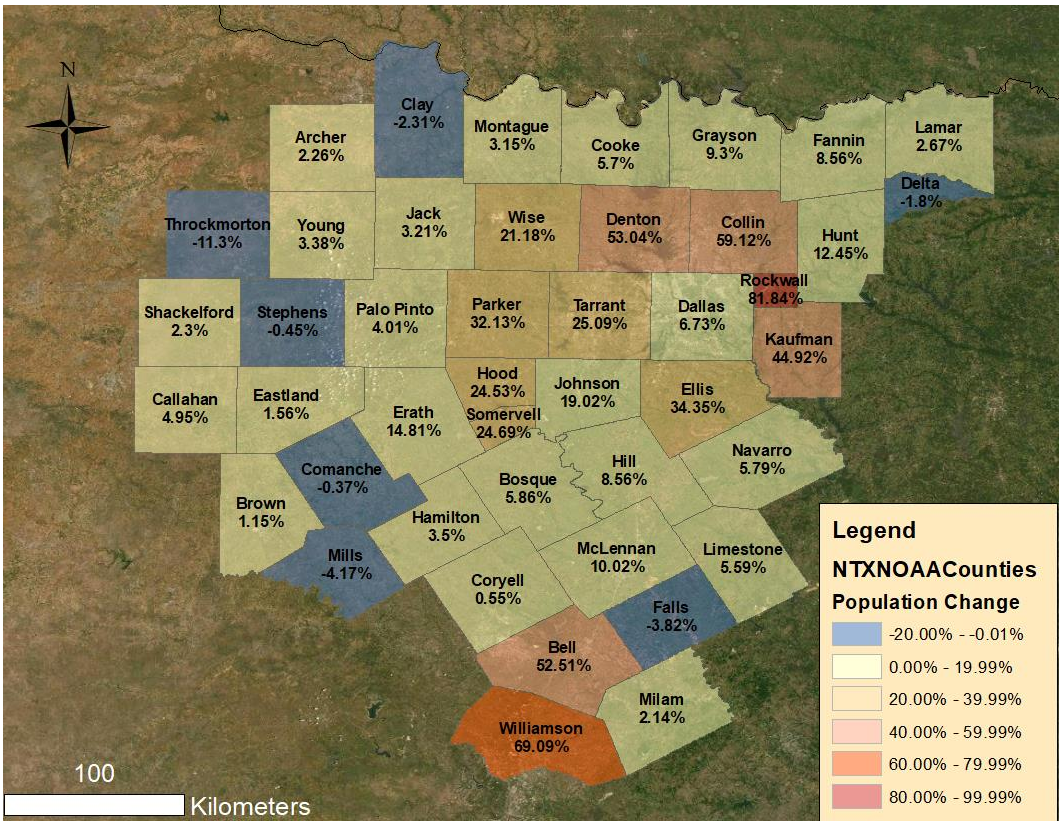

Figure 5: North Central Texas population change per county from 2000-2010. Population data courtesy of the U.S. Census Bureau.

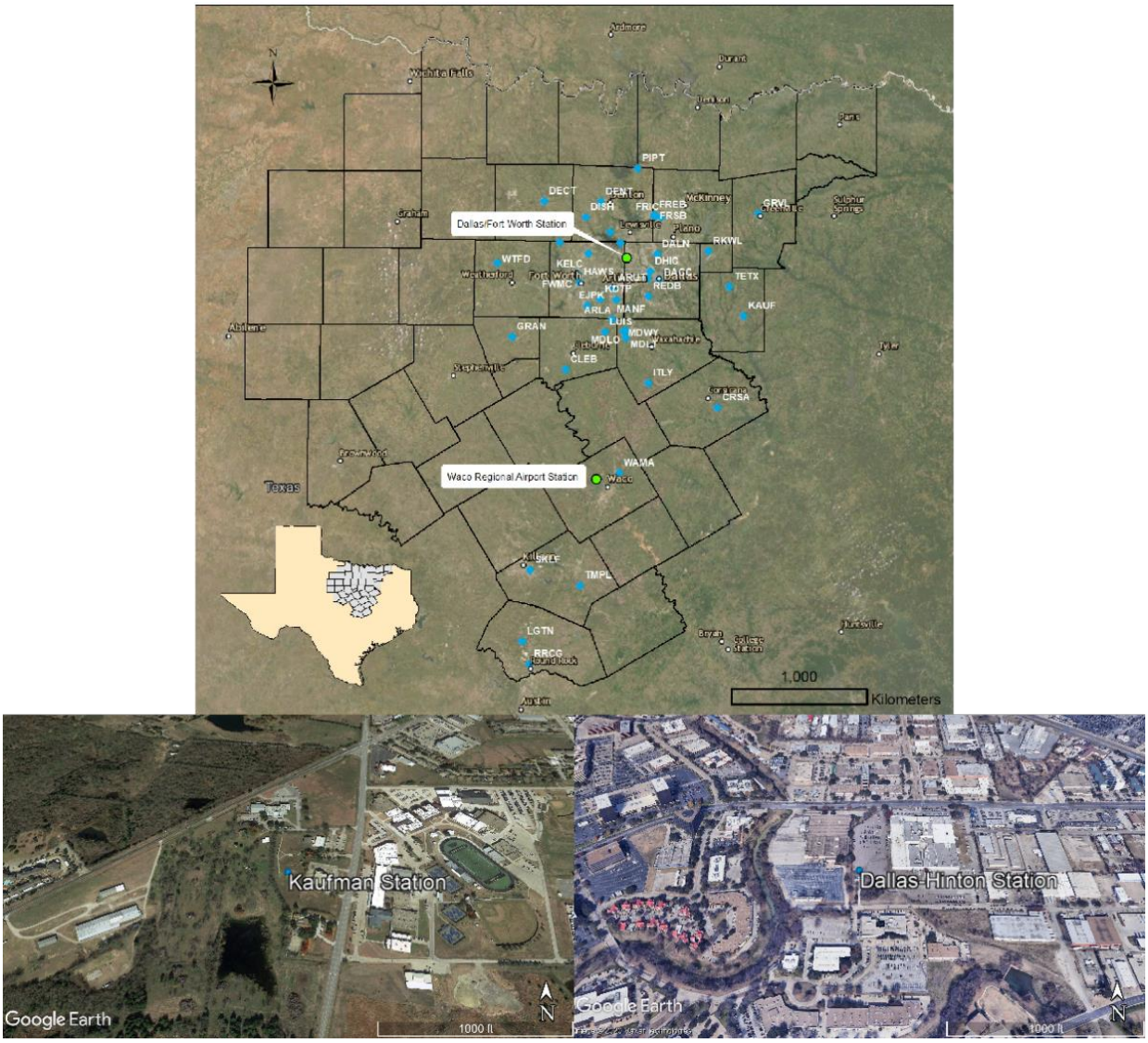

Figure 6: (Top) ArcGIS map of DFW and Waco NWS stations and 33 TCEQ CAMS stations, (bottom left) Kaufman CAMS station using Google Earth Pro 11-2018, (bottom right) Dallas-Hinton CAMS station using Google Earth Pro 10-2019.

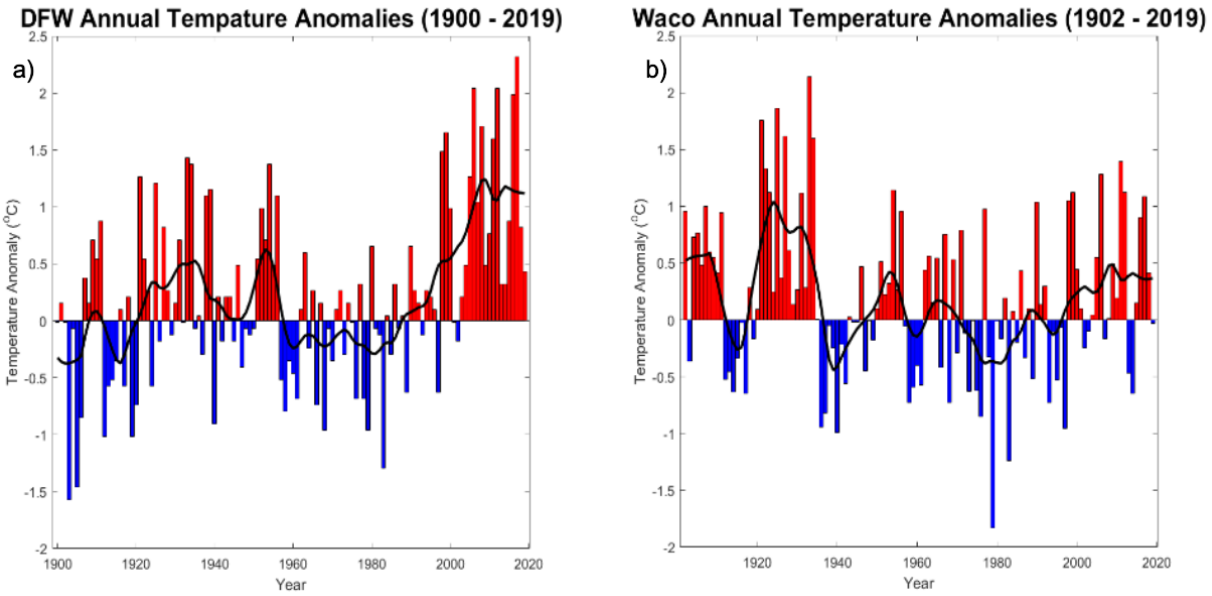

Figure 7: Temperature anomalies for (a) DFW and (b) Waco. A baseline average from 1951 – 1980 was used in accordance with GISS standards, and Lowess smoothing with a 25% span for trend interpretation.

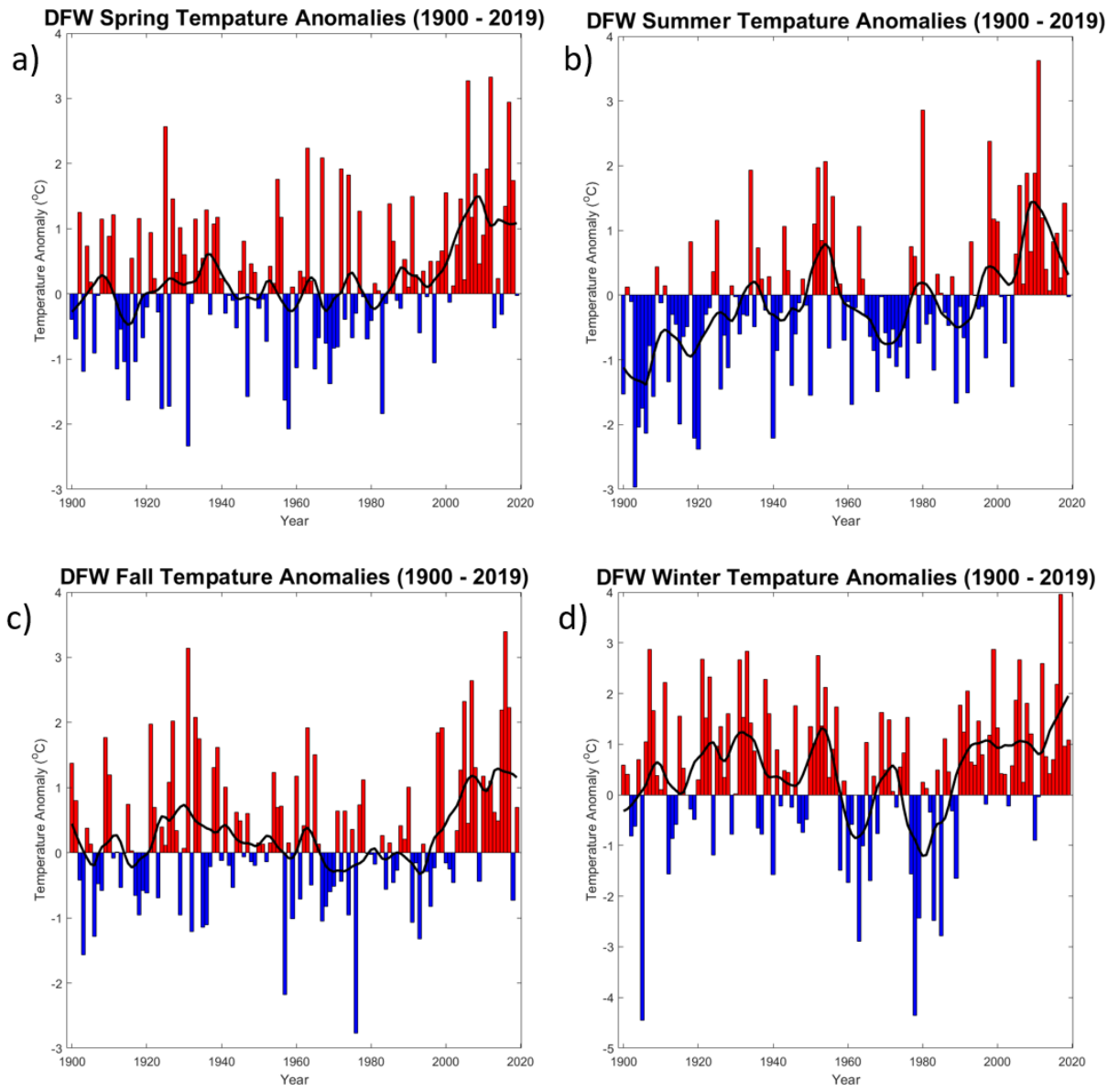

Figure 8: Seasonal average temperature anomalies for DFW with a) March, April, and May, b) June, July, and August, c) September, October, and November, and d) December, January, and February. A baseline average from 1951 – 1980 was used in accordance with GISS.

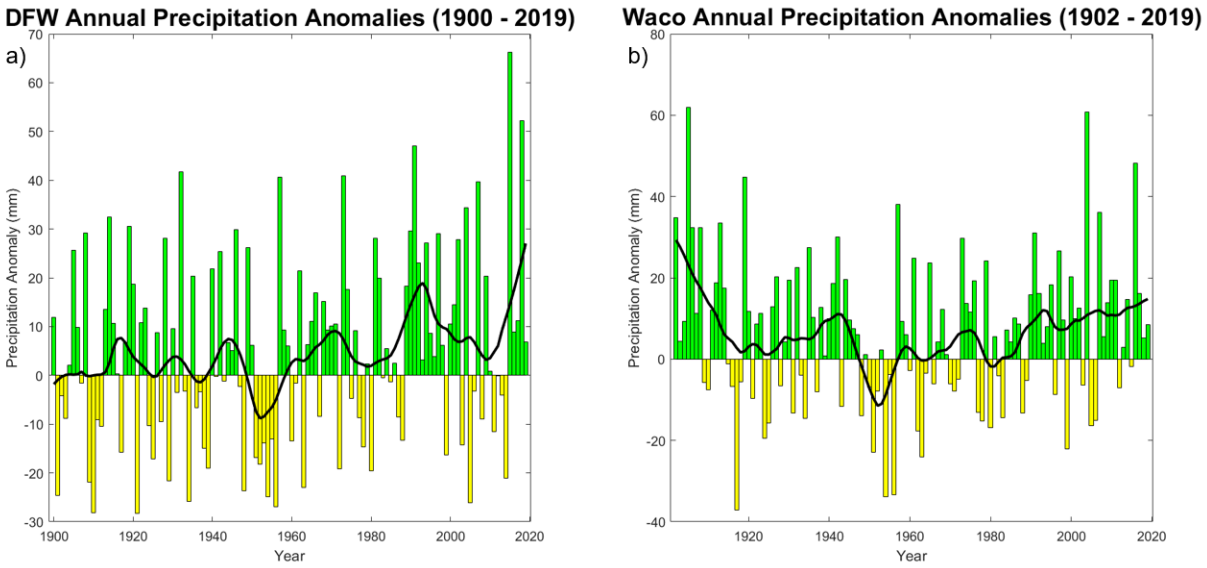

Figure 9: Precipitation anomalies for (a) DFW and (b) Waco. A baseline average from 1951 – 1980 was used in accordance with GISS standards, and Lowess smoothing with a 25% span for trend interpretation.

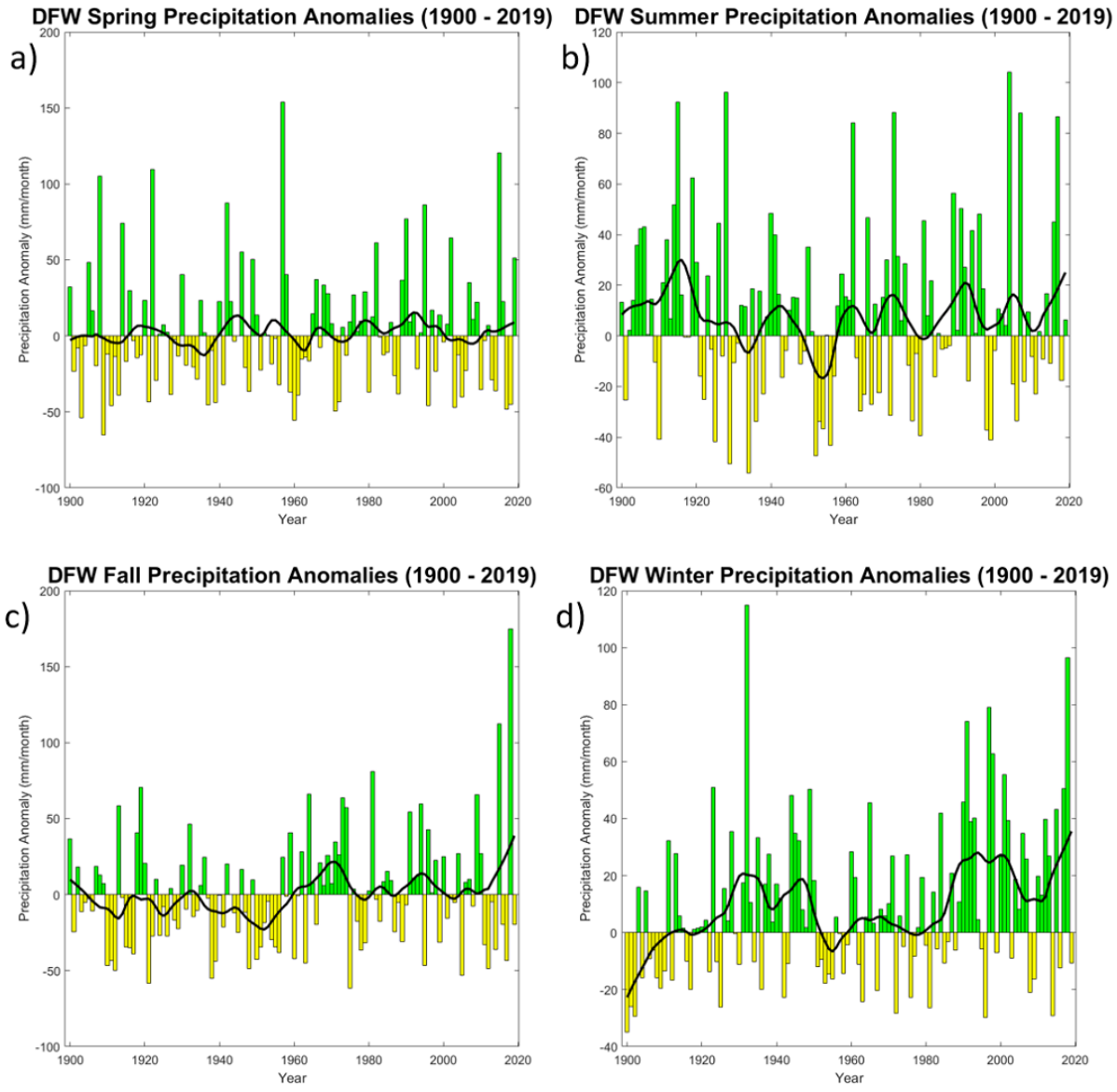

Figure 10: Seasonal average precipitation anomalies for DFW with a) March, April, and May, b) June, July, and August, c) September, October, and November, and d) December, January, and February. A baseline average from 1951 – 1980 was used in accordance with GIS

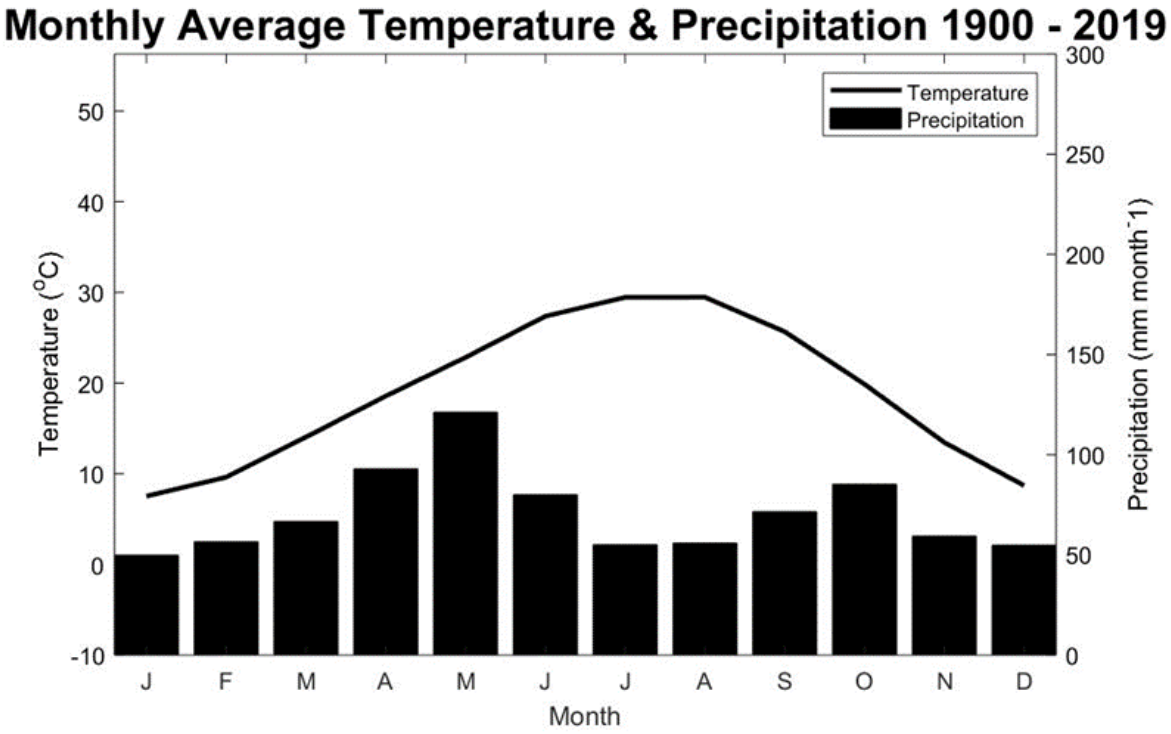

Figure 11: Average temperature and precipitation for the KDFW NWS station.

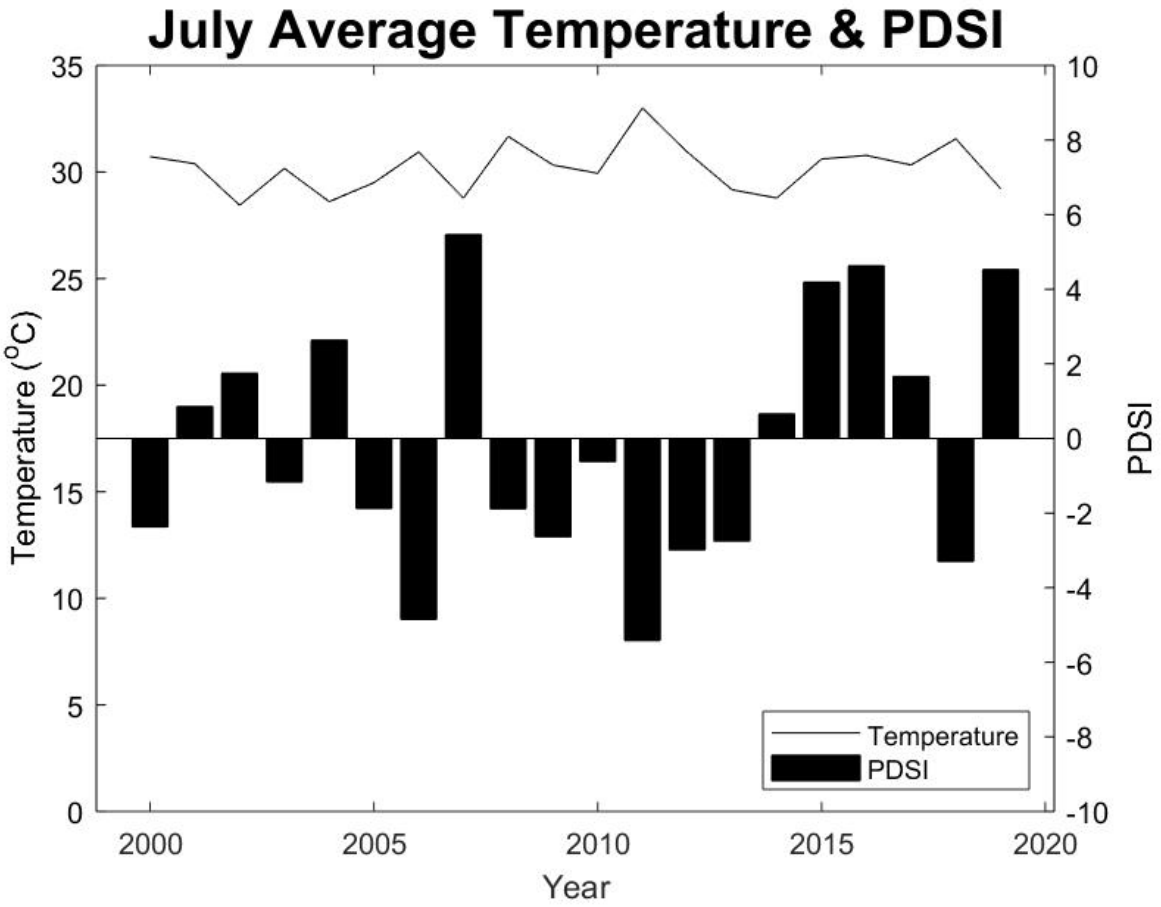

Figure 12: Average surface air temperature and PDSI for July from the KDFW NWS station.

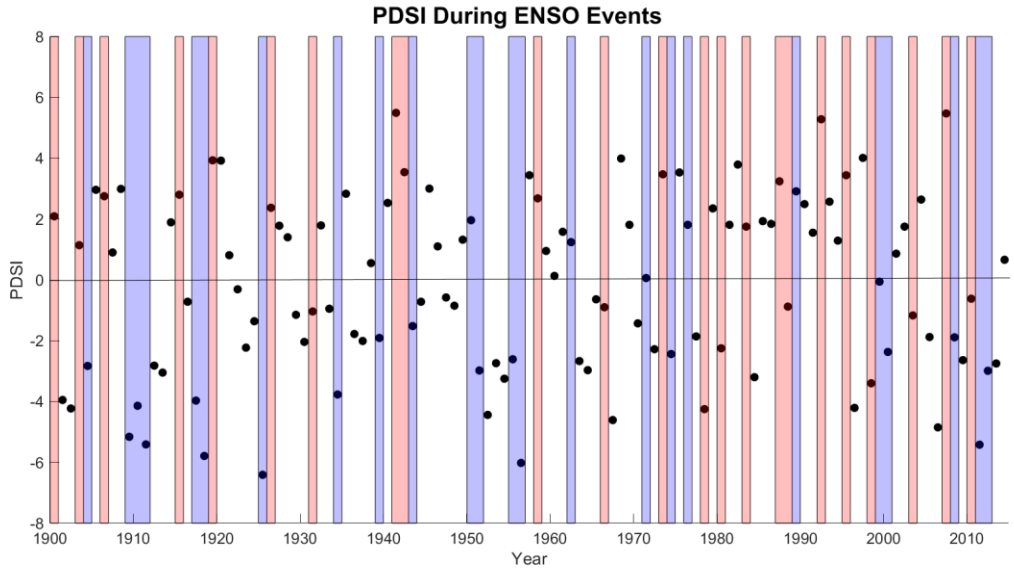

Figure 13: North Central Texas July PDSI overlayed on ENSO events during the time period of 1900 - 2015. Whereas, warm (red), cold(blue), and neutral(white) phases are indicated.

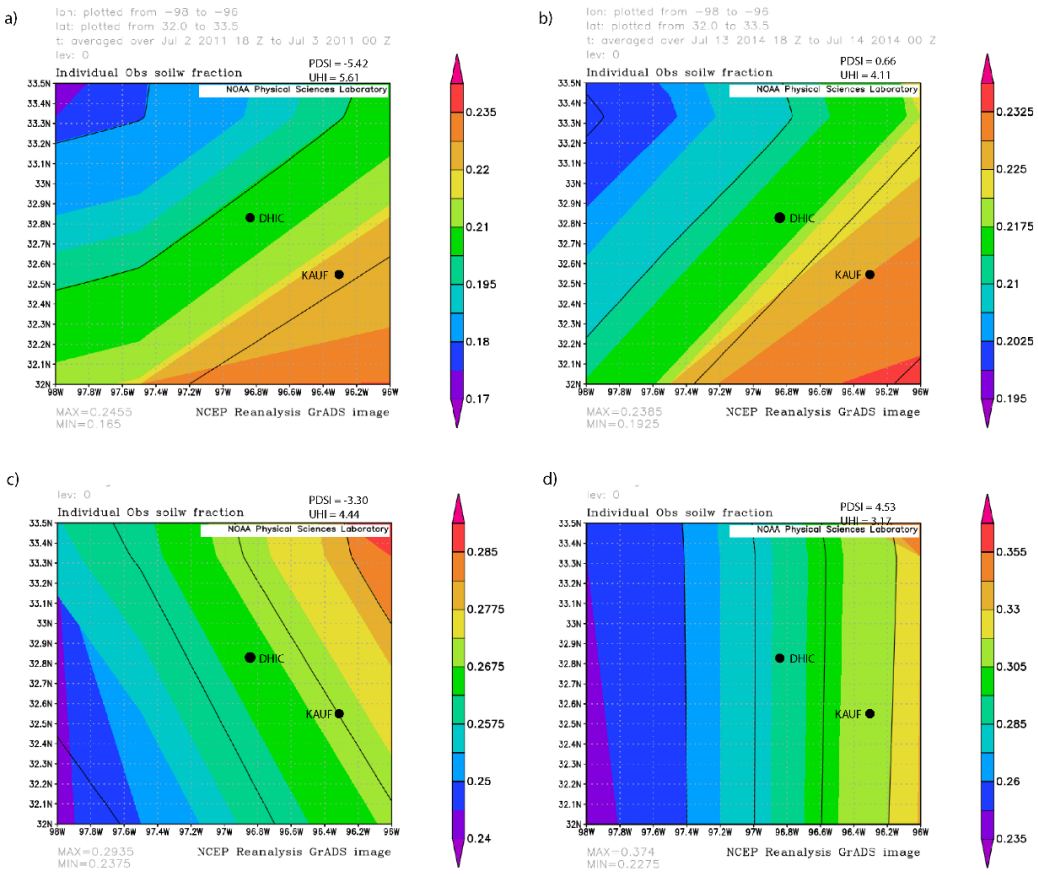

Figure 14: Volumetric soil moisture fraction in July for a) 2011 (extreme drought), b) 2014 (normal), c) 2018 (severe drought), and d) 2016 (extremely moist spell) from NCEP Reanalysis I for the DFW area. Measurements were obtained for days where the UHI magnitude was measured, and it should be noted that resolution is about 2° x 2°. Also shown are the approximate locations of the Dallas Hinton and the Kaufman TCEQ station.

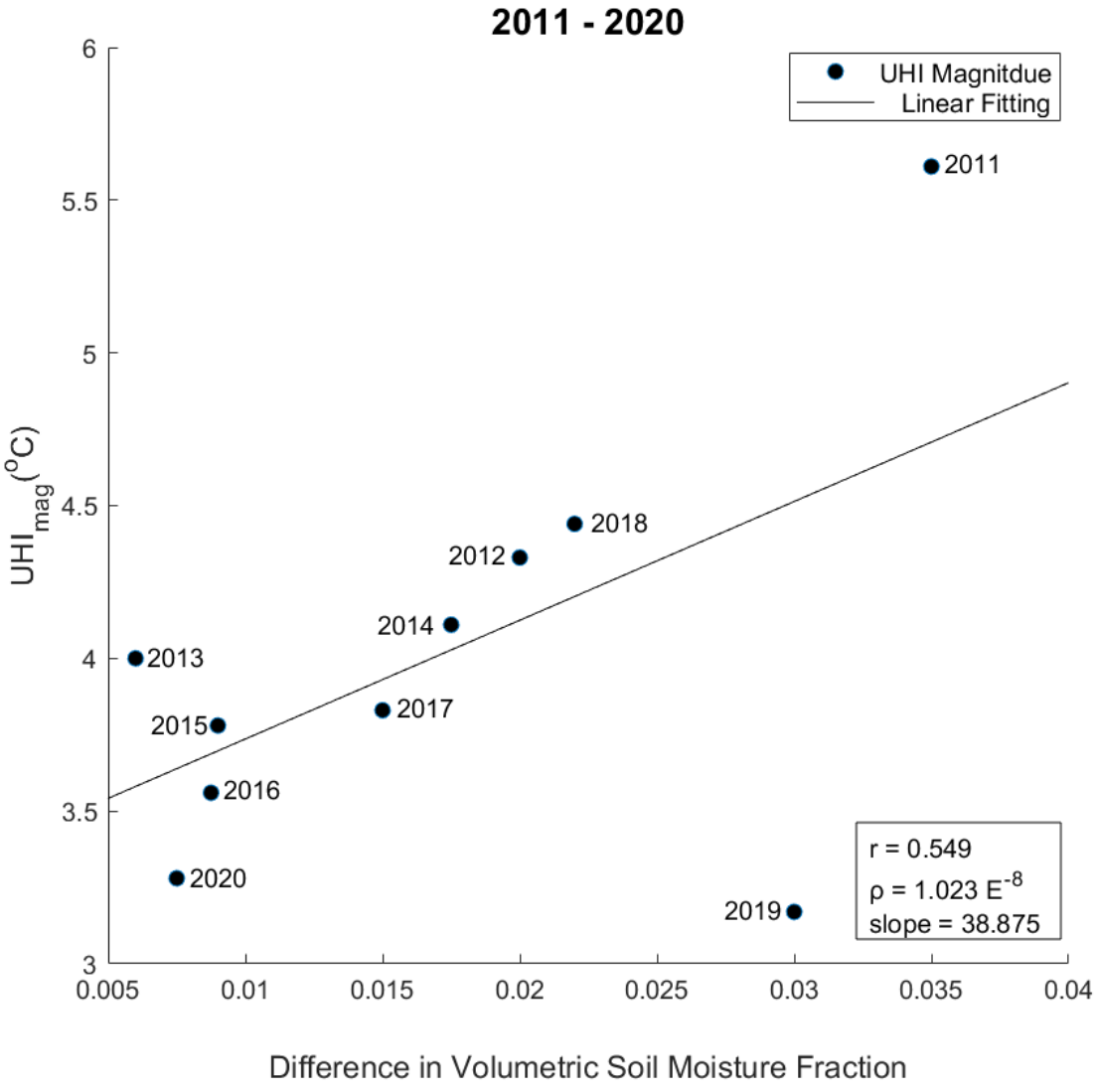

Figure 15: Approximate difference in the volumetric soil moisture fraction between the Kaufman rural site and Dallas-Hinton urban site using NCEP Reanalysis I and corresponding UHI_{mag}.

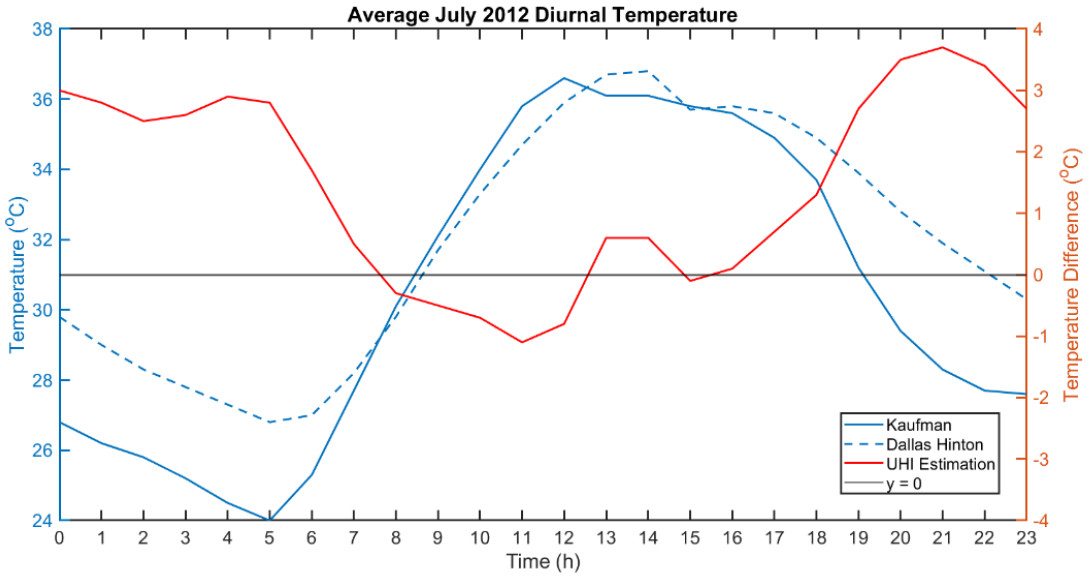

Figure 16: Diurnal temperature variation for the study urban and rural stations during all days with no precipitation and wind speed below 2 meters per second.

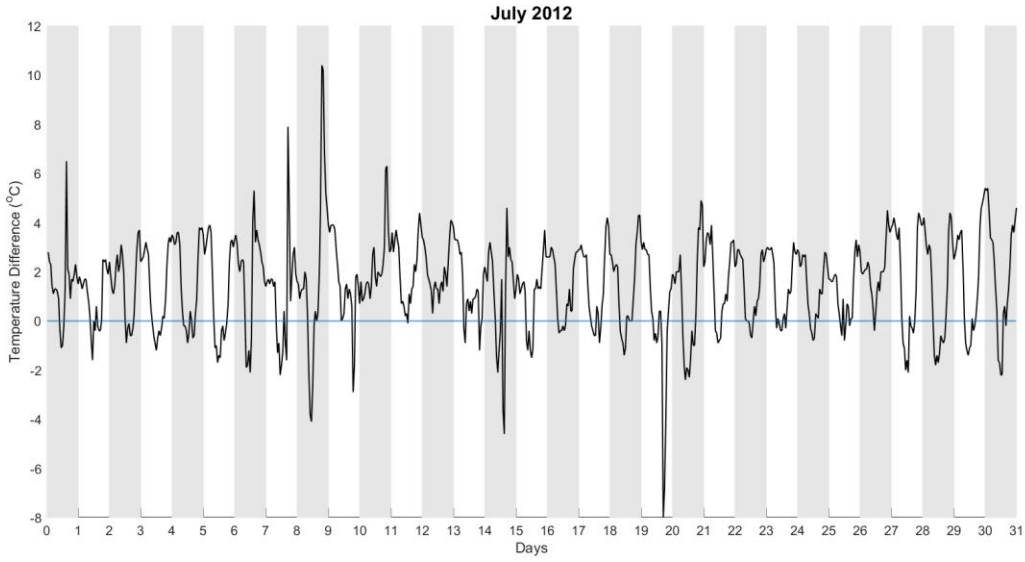

Figure 17: Temperature difference between the urban and rural stations for this study for the month of July 2012. Shaded and non-shaded areas represent a 24-hour period differentiating days.

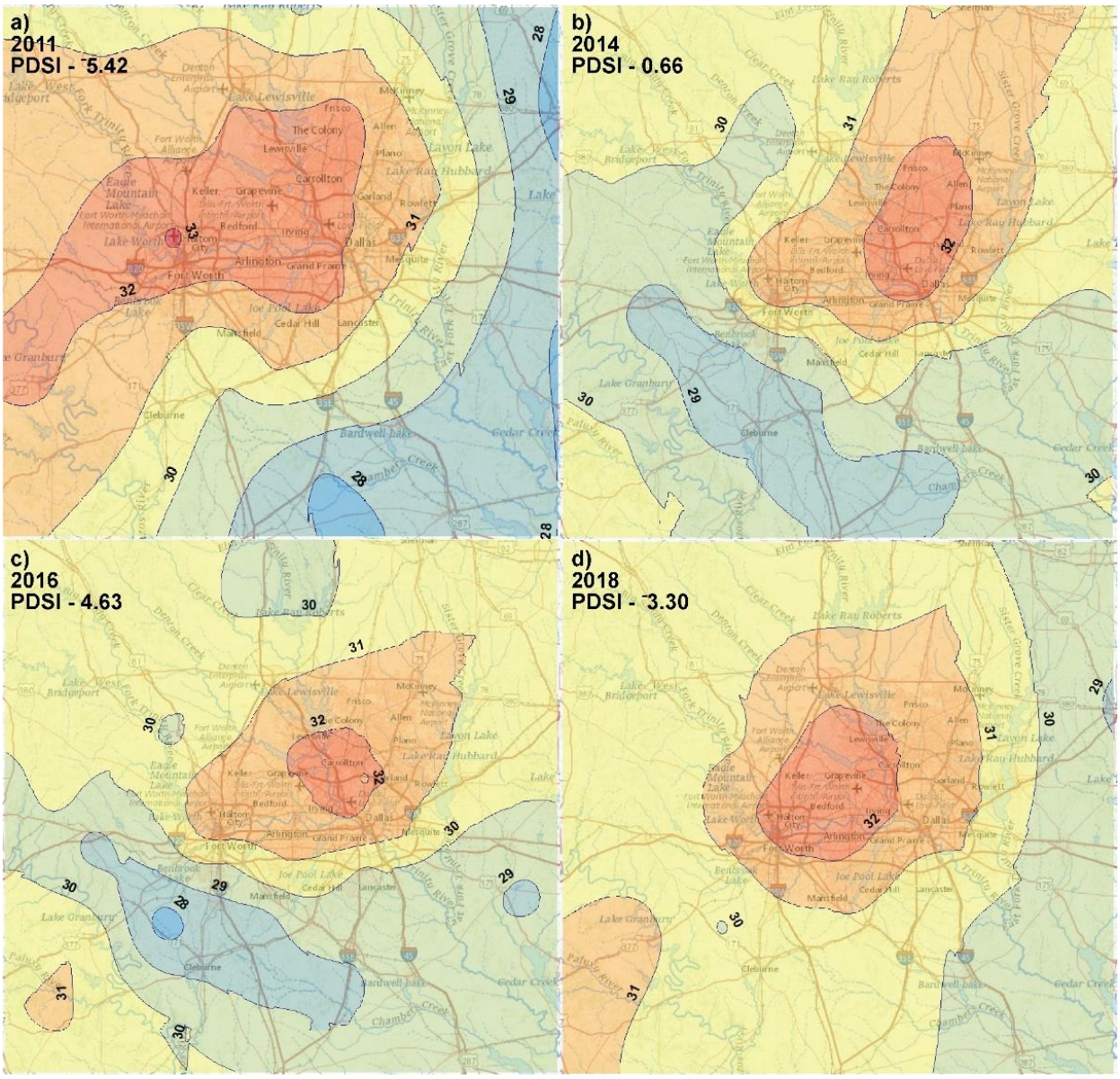

Figure 18: Temperature (°C) spatial distribution from TCEQ station, interpolated via ArcGIS Pro Kriging.

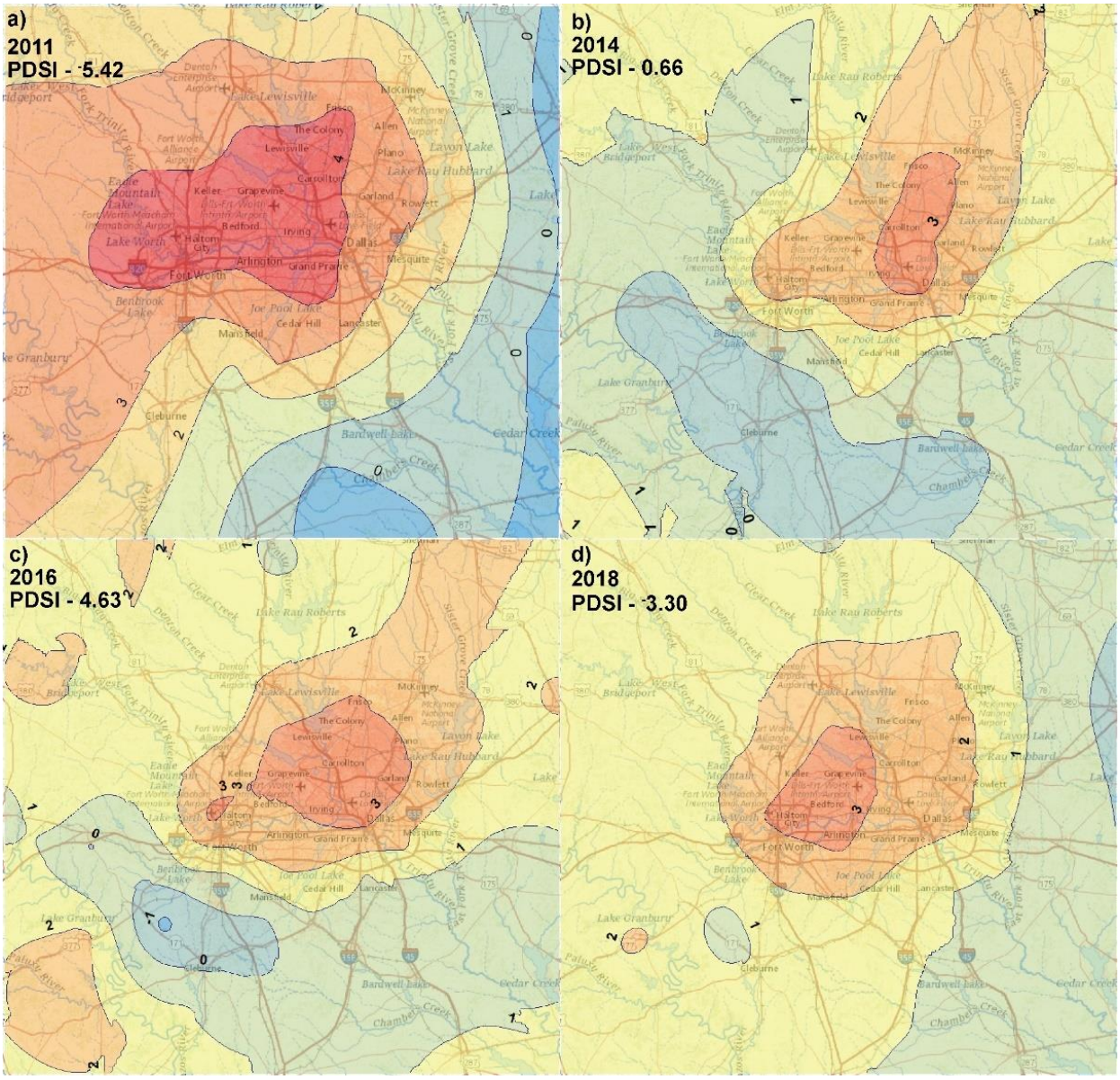

Figure 19: Temperature difference (°C) relative to the TCEQ station from Kaufman using ArcGIS Interpolation Kriging.

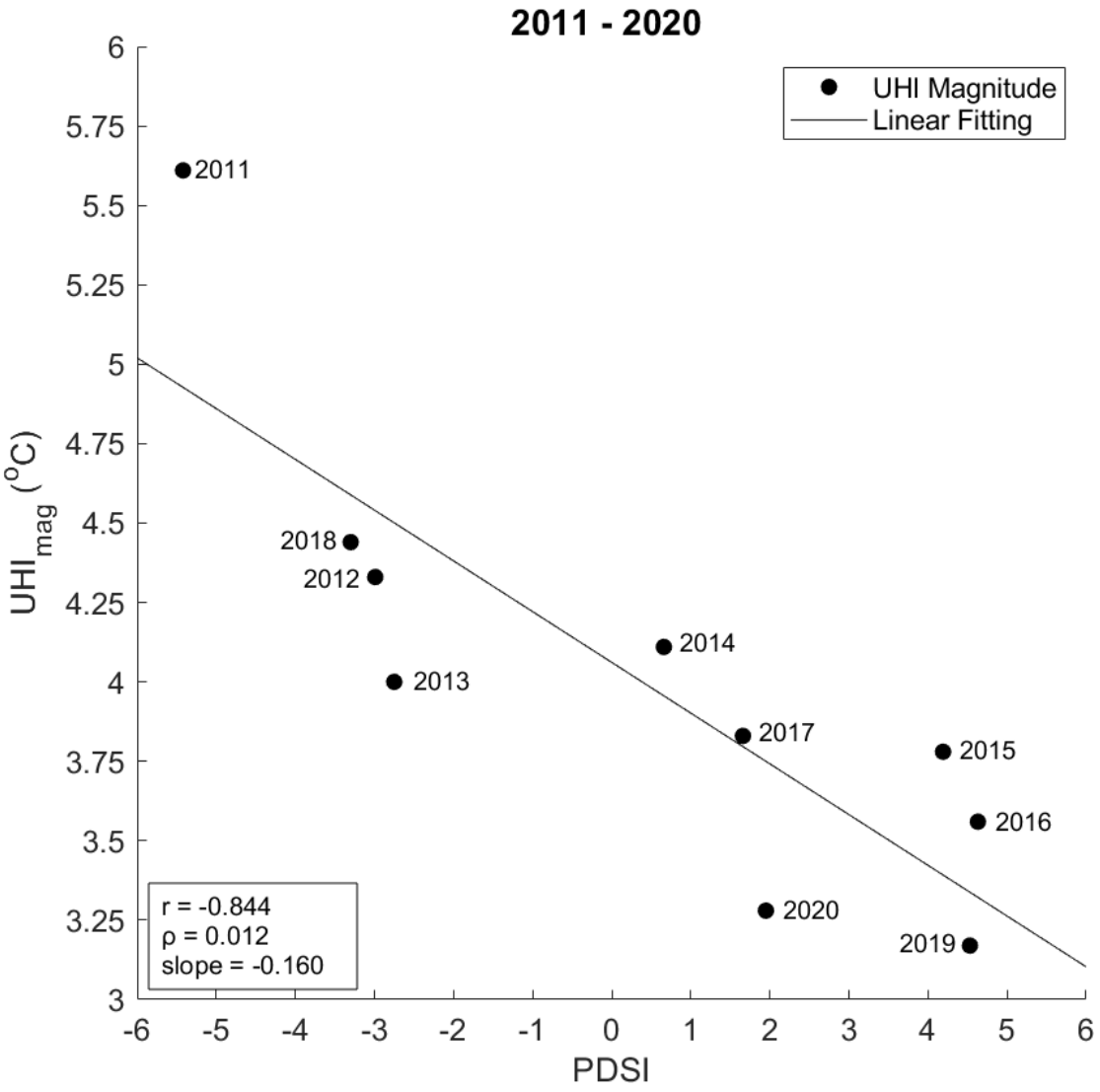

Figure 20: Palmer Drought Severity Index (PDSI) and UHI_{mag} for TCEQ Kaufman and Dallas Hinton stations at 21:00

References

Ackerman, B., 1985: Temporal March of the Chicago Heat Island. *J. Climate Appl. Meteor.*, **24**, 547–554, https://doi.org/10.1175/1520-0450(1985)024<0547:TMOTCH>2.0.CO;2.

Bai, Y., T. O. Ochuodho, and J. Yang, 2019: Impact of land use and climate change on water-related ecosystem services in Kentucky, USA. *Ecological Indicators*, **102**, 51–64, https://doi.org/10.1016/j.ecolind.2019.01.079.

Brandsma, T., and D. Wolters, 2020: Measurement and Statistical Modeling of the Urban Heat Island of the City of Utrecht (the Netherlands) - ProQuest. *ProQuest*,. https://search-proquest-com.ezproxy.uta.edu/docview/1022276078?pq-origsite=summon (Accessed July 10, 2020).

Bjerknes, J., 1969: ATMOSPHERIC TELECONNECTIONS FROM THE EQUATORIAL PACIFIC. *Monthly Weather Review*, **97**, 163–172, https://doi.org/10.1175/1520-0493(1969)097<0163:ATFTEP>2.3.CO;2.

Cleveland, W. S., 1979: Robust Locally Weighted Regression and Smoothing Scatterplots. *Journal of the American Statistical Association*, **74**, 829–836, https://doi.org/10.1080/01621459.1979.10481038.

Data.GISS: GISS Surface Temperature Analysis (v4): Analysis Graphs and Plots. https://data.giss.nasa.gov/gistemp/graphs_v4/ (Accessed September 21, 2020).

U.S. Census Data. *United States Census Bureau*, https://data.census.gov/cedsci/ (Accessed September 21, 2020).

Foster, G., and S. Rahmstorf, 2011: Global temperature evolution 1979–2010. *Environ. Res. Lett.*, **6**, 044022, https://doi.org/10.1088/1748-9326/6/4/044022.

Hansen, J., R. Ruedy, J. Glascoe, and M. Sato, 1999: GISS analysis of surface temperature change. *J. Geophys. Res.*, **104**, 30997–31022, https://doi.org/10.1029/1999JD900835.

Hoerling, M., A. Kumar, R. Dole, J.W. Nielsen-Gammon, J. Eischeid, J. Perlwitz, X.W. Quan, T. Zhang, P. Pegion, and M. Chen, 2013: Anatomy of an Extreme Event. *Journal of Climate*, **26**, 2811–2832, https://doi.org/10.1175/JCLI-D-12-00270.1.

Howard, L., 1833: *The climate of London*. Vols. 1-3. Harvey and Dorton, 1002 pp.

Hu, X.-M., and M. Xue, 2016: Influence of Synoptic Sea-Breeze Fronts on the Urban Heat Island Intensity in Dallas–Fort Worth, Texas. *Monthly Weather Review*, **144**, 1487–1507, https://doi.org/10.1175/MWR-D-15-0201.1.

Hu, X.-M., M. Xue, P. M. Klein, B. G. Illston, and S. Chen, 2016: Analysis of Urban Effects in Oklahoma City using a Dense Surface Observing Network. *Journal of Applied Meteorology and Climatology*, **55**, 723–741, https://doi.org/10.1175/JAMC-D-15-0206.1.

IPCC, 2013: Climate Change 2013: The Physical Science Basis. Contribution of Working Group I to the Fifth Assessment Report of the Intergovernmental Panel on Climate Change [Stocker, T.F., D. Qin, G.-K. Plattner, M. Tignor, S.K. Allen, J. Boschung, A. Nauels, Y. Xia, V. Bex and P.M. Midgley (eds.)]. Cambridge University Press, Cambridge, United Kingdom and New York, NY, USA, 1535 pp, doi:10.1017/CBO9781107415324.

Kalnay, E., and Coauthors, 1996: The NCEP/NCAR 40-Year Reanalysis Project. *Bulletin of the American Meteorological Society*, **77**, 437–471.

Khedun, C. P., A. K. Mishra, V. P. Singh, and J. R. Giardino, 2014: A copula-based precipitation forecasting model: Investigating the interdecadal modulation of ENSO's impacts on monthly precipitation. *Water Resources Research*, **50**, 580–600, https://doi.org/10.1002/2013WR013763.

Kurtzman, D., and B. R. Scanlon, 2007: El Niño–Southern Oscillation and Pacific Decadal Oscillation impacts on precipitation in the southern and central United States: Evaluation of spatial distribution and predictions. *Water Resources Research*, **43**, https://doi.org/10.1029/2007WR005863.

Lawrence, D. M., and Coauthors, 2019: The Community Land Model Version 5: Description of New Features, Benchmarking, and Impact of Forcing Uncertainty. *Journal of Advances in Modeling Earth Systems*, **11**, 4245–4287, https://doi.org/10.1029/2018MS001583.

Liu, J., and D. Niyogi, 2020: Identification of linkages between urban heat Island magnitude and urban rainfall modification by use of causal discovery algorithms. *Urban Climate*, **33**, 100659, https://doi.org/10.1016/j.uclim.2020.100659.

McCabe, G. J., and M. D. Dettinger, 1999: Decadal variations in the strength of ENSO teleconnections with precipitation in the western United States. *International Journal of Climatology*, **19**, 1399–1410, https://doi.org/10.1002/(SICI)1097-0088(19991115)19:13<1399::AID-JOC457>3.0.CO;2-A.

Molles, M. C., 2013: *Ecology: concepts and applications*, McGraw-Hill, 567pp.

Nielsen-Gammon, J.W., 2011: The changing climate of Texas. *The Impact of Global Warming on Texas,* G.R. North, J. Schmandt, and J. Clarkson, Eds., University of Texas Press, 39-86.

NOAA National Centers for Environmental Information, 2020: State of the Climate: Global Climate Report for Annual 2019, retrieved on January 16, 2020 from https://www.ncdc.noaa.gov/sotc/global/201913.

Oke, T.R., 1973: City size and the urban heat island. *Atmos. Environ.,* **7,** 769-779.

Oke, T. R., 1976: The distinction between canopy and boundary-layer urban heat islands. *Atmosphere*, **14**, 268–277, https://doi.org/10.1080/00046973.1976.9648422.

Oke, T.R., 1982: The energetic basis of the urban heat island. *Quart. J. Roy. Meteor. Soc.,* **108,** 1-24.

Oke, T. R., and G. B. Maxwell, 1975: Urban heat island dynamics in Montreal and Vancouver. *Atmos. Environ.* **9**, 191–200, https://doi.org/10.1016/0004-6981(75)90067-0.

Oke, T. R., G. Mills, A. Christen, and J. A. Voogt, 2017: *Urban Climates*. Cambridge University Press,.

Palmer, W., 1965: Meteorological Drought. Research paper no.45, U.S. Department of Commerce Weather Bureau, February 1965, 58 pp. Available online by the NOAA National Climatic Data Center at http://www.ncdc.noaa.gov/temp-and-precip/drought/docs/palmer.pdf

Romero-Lankao, P., J.B. Smith, D.J. Davidson, N.S. Diffenbaugh, P.L. Kinney, P. Kirshen, P. Kovacs, and L. Villers Ruiz, 2014: North America. In: Climate Change 2014: Impacts, Adaptation, and Vulnerability. Part B: Regional Aspects. Contribution of Working Group II to the Fifth Assessment Report of the Intergovernmental Panel on Climate Change [Barros, V.R., C.B. Field, D.J. Dokken, M.D. Mastrandrea, K.J. Mach, T.E. Bilir, M. Chatterjee, K.L. Ebi, Y.O. Estrada, R.C. Genova, B. Girma, E.S. Kissel, A.N. Levy, S. MacCracken, P.R. Mastrandrea, and L.L.White (eds.)]. Cambridge University Press, Cambridge, United Kingdom and New York, NY, USA, pp. 1439-1498

Roth, M., 2007: Review of urban climate research in (sub)tropical regions. *International Journal of Climatology*, **27**, 1859–1873, https://doi.org/10.1002/joc.1591.

Roxon, J., F.-J. Ulm, and R. J.-M. Pellenq, 2020: Urban heat island impact on state residential energy cost and CO2 emissions in the United States. *Urban Climate*, **31**, 100546, https://doi.org/10.1016/j.uclim.2019.100546.

Runnalls, K.E., and T.R. Oke, 2000: Dynamics and controls of the near-surface heat island of Vancouver, British Columbia. *Phys. Geogr.* **21,** 283-304.

Schmidlin, T. W., 1989: The Urban Heat Island at Toledo, Ohio. *Ohio Journal of Science,* **89**, 38-41.

Seager, R., L. Goddard, J. Nakamura, N. Henderson, and D. E. Lee, 2014: Dynamical Causes of the 2010/11 Texas–Northern Mexico Drought. *Journal of Hydrometeorology*, **15**, 39–68, https://doi.org/10.1175/JHM-D-13-024.1.

TCEQ, cited 2021: TCEQ air and water monitoring station. Texas Commission for Environmental Quality. [Available online at http://www.tceq.texas.gov/cgi-bin/compliance/monops/daily_summary.pl.]

Wagner, P., and K. Schäfer, 2017: Influence of mixing layer height on air pollutant concentrations in an urban street canyon. *Urban Climate*, **22**, 64–79, https://doi.org/10.1016/j.uclim.2015.11.001.

Wentz, F. J., L. Ricciardulli, K. Hilburn, and C. Mears, 2007: How Much More Rain Will Global Warming Bring? *Science*, **317**, 233–235.

Winguth, A. M. E., and B. Kelp, 2013: The Urban Heat Island of the North-Central Texas Region and Its Relation to the 2011 Severe Texas Drought. *Journal of Applied Meteorology and Climatology*, **52**, 2418–2433.

You H, L. Potter, L. Valencia, S. Robinson, 2019: Texas Population Projections 2010 to 2050. Texas Demographic Center. 28 May 2020, https://demographics.texas.gov/Resources/publications/2019/20190128_PopProjectionsBrief.pdf

Zhang, X., G.-J. Steeneveld, D. Zhou, C. Duan, and A. A. M. Holtslag, 2019: A diagnostic equation for the maximum urban heat island effect of a typical Chinese city: A case study for Xi'an. *Building and Environment*, **158**, 39–50, https://doi.org/10.1016/j.buildenv.2019.05.004.

Biographical Information

Linnea Standard has a Bachelor of Science degree in Biology, a Master Certification in Geographic Information Systems, and a Master of Science degree in Earth and Environmental Science from the University of Texas Arlington. Her GIS certification included working with the city of Fort Worth on increasing housing and support infrastructure from previously developed land. Linnea's thesis project entailed the DFW metroplex urban heat island and its relationship with regional drought.